Chapter 4

Real-time manganese phase dynamics during abiotic and biological manganese oxide reduction

Jena E Johnson[1], Pratixa Savalia[2], Ryan Davis[3], Benjamin Kocar[4], Samuel M Webb[3], Kenneth Nealson[2], Woodward W Fischer[1]

[1]Division of Geological and Planetary Sciences, California Institute of Technology, Pasadena, CA 91125, USA. [2]University of Southern California, Los Angeles, CA 90089. [3]Stanford Synchrotron Radiation Lightsource, Menlo Park CA 94025. [4]Massachusetts Institute of Technology, Cambridge MA 02139.

ABSTRACT

Many toxic and bioessential trace elements are sequestered by insoluble manganese oxides, but Mn oxides are also highly reactive and easily reduced by a variety of species, abiotically and as a part of biological anaerobic respiration. The reaction pathways during these different manganese oxide reduction routes and their products have been thusfar understudied. We measured the sequence progression of live microbial manganese(IV) oxide reduction under several environmentally-relevant conditions using real-time synchrotron x-ray spectroscopic measurements and x-ray diffraction on precipitates collected throughout the reaction. These results were compared to abiotic reduction pathways using common inorganic reductants sulfide and ferrous iron. We observed formation of rhodochrosite ($MnCO_3$) during the microbial reduction of Mn(IV) oxides with high organic carbon and negligible phosphate while high phosphate and organic carbon conditions formed Mn(II)-phosphate. Both sulfide and ferrous iron reduction of manganese oxides in the

absence of inorganic carbon produced only aqueous Mn^{2+}. A Mn(III) oxyhydroxide intermediate similar to feitknechtite was produced during sulfide- and ferrous iron-induced reduction and during low-phosphate experiments, which we suggest was formed during comproportionation reactions between remnant Mn(IV) oxides and produced Mn^{2+}. Our real-time measurements contribute to understanding the kinetics and mechanism of Mn(IV) oxides reduction and what the possible mineralogical intermediates and products are, and our observations should assist in interpreting the processes recorded in the geologic record of manganese on Earth and beyond.

INTRODUCTION

The cycling of manganese is critically important for the sequestration of toxins and trace metals, the neutralization of reactive oxygen species and the reactivity of major geochemical species like sulfur and iron[1]. Manganese is introduced to the fluid Earth as soluble Mn^{2+} by hydrothermal sources or igneous rock weathering but is oxidized in oxygenated water and air to insoluble Mn(III,IV) oxyhydroxides[2–4]. These manganese oxides are highly favorable electron acceptors for microbial anaerobic respiration[5,6], an important process both in marine sediments and terrestrial environments[7–9]. But manganese can also be rapidly reduced by many inorganic species, including ferrous iron, sulfide, arsenite and uraninite[10–13]. These Mn(III,IV) oxides are then deposited in sediments, where they are often rapidly cycled as they undergo many reduction and re-oxidation reactions[1,8].

Initial manganese precipitates can be subsequently incorporated into the sedimentary record or aqueous manganese(II) can be released to shallower sediments, groundwater, or other nearby fluids. Currently, it is unclear which reductants and what environmental conditions control the behavior of manganese and its potential to become 'fixed' in minerals or re-released. The geologic record of manganese is illuminating here:
while manganese is deposited primarily as Mn(IV) oxides [1,14–19], ancient well-preserved sedimentary rocks host Mn in more reduced phases, mainly in Mn-bearing carbonates [rhodochrosite, $MnCO_3$, or kutnohorite, $Mn_{0.5}Ca_{0.5}CO_3$] or in Mn(II,III) silicified oxides [braunite, $Mn(III)_6Mn(II)SiO_{12}$] [3,20–23]. These Mn-carbonates have been hypothesized to be derived from Mn(IV) oxides undergoing post-depositional diagenetic reduction by organic carbon (microbially-mediated at low-temperatures) [3,22–25], as in Rxn 1 and 2:

$$2\ Mn(IV)O_2 + CH_2O + 4\ H^+ \rightleftharpoons 2\ Mn^{2+} + CO_2 + 3\ H_2O \quad (1)$$

$$Mn^{2+} + CO_3^{2-} \rightleftharpoons MnCO_3 \quad (2)$$

However, the high redox potential of manganese results in multiple possible Mn(IV) reduction pathways, including but not limited to microbially-mediated reactions with organic carbon. The mechanistic differences and the mineralogical products of the various Mn reduction potential pathways have been understudied. Rhodochrosite has been observed as a product of microbial respiration of Mn oxides previously[5,12,26] although not explored extensively for the requisite conditions of precipitation. Other

studies have measured Mn-carbonate production during microbial sulfate reduction or thiosulfate disproportionation from secondary abiotic interactions between sulfide and Mn-oxides [27–30].

To our knowledge only one study has measured a partial reaction sequence of Mn(IV) oxides to Mn(II)-carbonate, using time-resolved XRD measurements [31]. Fischer et al. reacted total membrane extracts from *Shewanella oneidensis* with powdered birnessite (a layered Mn(III,IV) oxide) and observed the mineralogical changes that occurred, reportedly finding production of rhodochrosite and hausmannite (Mn_3O_4), although only rhodochrosite data is shown. However, using only XRD measurements limits the results to crystalline phases, and it is unclear how much this *in vitro* study really represents natural reaction mechanisms and mineralogical changes.

Our experiments seek to systematically address what the environmental and mechanistic controls are on mineral products of Mn oxide reduction with various reductants. Time-resolved measurements both constrain the reduction mechanism and reveal reaction intermediates during various Mn reduction pathways. These intermediates may be stabilized as products if Mn reduction is reductant-limited, introducing another set of possible products. Real-time measurements of the Mn redox state and phase throughout inorganic and organic, microbially-mediated manganese reduction reveals the reaction mechanisms for these two distinct processes. Not only do these experiments yield mechanistic insight, but we can also compare reaction intermediates and products for

different reduction pathways against observations from Earth's modern environments and ancient rock record.

MATERIALS AND METHODS

Abiotic and biologically-mediated manganese reduction reactions were analyzed using a succession of X-ray spectroscopic measurements to assess what manganese phases were formed throughout the reaction. Measuring the dynamics of manganese phase changes *in situ* is highly challenging because of the complex media necessary for microbial sustenance, the amorphous intermediate phases often formed in low-temperature reactions, and (during microbial experiments) the extra complications introduced by cellular mass. These issues make real-time measurements not feasible by Raman, Fourier Transform Infrared Spectroscopy, or X-ray Diffraction (XRD) techniques, although these methods can and do help to assess crystalline products. X-ray absorption spectroscopy (XAS) is the ideal way to probe the entire reaction sequence since XAS can focus on one element (Mn) without matrix effects and measure the coordination and redox environment of all phases (contributing at least 5% to the total) regardless of crystallinity[32]. Thus all experiments were performed at the Stanford Synchrotron Radiation Lightsource, either on beam line 11-2 or beam line 4-1. We used high concentrations of Mn oxides and large quantities of bacteria to have strong Mn signal and rapid enough rates to measure in limited synchrotron time. This does not mimic environments directly, but reveals how these reactions progress mechanistically.

To capture the reduction reaction in real-time, we set up a flow-through system which siphoned a subsample of a stirred 1L reaction vessel into a small flow cell where the X-ray beam could evaluate the Mn valence state and coordination environment (Figure 1). Our flow-through cell was constructed from polymethacrylate polymer using a 3D printer. Fluid moved rapidly through the tubing and flow through cell and we saw no evidence of beam reduction or lactate-induced reduction in multi-hour control experiments with 20mM lactate and Mn oxides (Figure S1). New X-ray absorption spectra to detect Mn coordination and redox state (see [23,33–35]) were measured every 20 to 30 minutes. The reaction vessel was sealed with a rubber stopper and anaerobic conditions were maintained by nitrogen gas inflow. Solid filter samples were taken using a sampling portal through the rubber stopper and later analyzed using synchrotron-based x-ray diffraction on beam line 11-3 to characterize crystalline products and confirm XAS identifications.

Our reaction vessel contained the M1 minimal media (after Kostka and Nealson[36], with phosphate eliminated unless noted) necessary for our biotic experiments, 20mM lactate except in a lactate-limiting experiment, and began with freshly-made colloidal $Mn(IV)O_2$. For each experiment, we prepared colloidal MnO_2 by mixing equal weights of potassium permanganate and sodium thiosulfate (~1g each, after Perez-Benito et al, 1989) in a small volume of milliQ water (~20mL) and washed once with a dilute sodium chloride solution (.008M NaCl) to remove any adsorbed sulfur species, pipetting away as much excess solution as possible. We added this colloidal MnO_2 to the reaction vessel in an anaerobic

chamber. Using colloidal MnO_2 reduced the experimental time dramatically, since non-crystalline Mn(IV) oxides are much more reactive than crystalline Mn(IV) oxides like birnessite or pyrolusite, but this did add some variety to our initial conditions. Our media was always titrated to pH 8, but with the colloidal MnO_2 addition, occasionally additional pH adjustments were necessary (using sodium hydroxide or hydrochloric acid) to return the initial pH to 8.

For our microbially-mediated manganese reduction experiments, we used a wild-type bacterial system to most realistically capture the process dynamics of Mn reduction. We chose to use *Shewanella oneidensis,* a well-studied model bacteria for anaerobic metal reduction including the reduction of Mn(IV) oxides [11,37–39]. *S. oneidensis* employs either (or both) soluble electron carriers [flavins][40,41] or direct electron transfer on the cell surface or via nanowires [42–44] to pass electrons from a limited number of organic compounds to a substantial diversity of electron acceptors. Regardless of the mechanism, the reduction reaction should be similar for *Shewanella* and other microbial manganese reducers:

$$2\ Mn(IV)O_2 + C_3H_5O_3^- + 4\ H^+ \rightleftharpoons 2\ Mn^{2+} + C_2H_3O_2^- + CO_2 + 3\ H_2O \qquad (3)$$

[lactate] *[acetate]*

This reaction produces reduced manganese, alkalinity, and dissolved inorganic carbon, which should promote the precipitation of manganese carbonates [3,45].

We grew *S. oneidensis* in conditions to optimize cellular density so the experiments could be performed in limited time spans. *S. oneidensis* was grown aerobically in Lysogeny Broth (LB) in a 25-30°C shaking incubator until the optical density at 600nm was approximately 1.2. We then spun down the cells in 250mL tubes using a centrifuge at 3000rpm for 5 minutes and resuspended the cells in a small amount of LB. The thick cellular paste (often 10-15mL) was added to the reaction vessel through the sampling port by a syringe after acquiring an initial MnO_2 spectra.

We performed three variations of microbially-mediated reduction of Mn(IV) oxides. One had our 'normal' conditions of being lactate-replete (20mM) but no added phosphate in the media, so the bacteria only had the cellular phosphate they had accumulated while growing in LB. Another had similarly phosphate-restricted conditions but also was limiting in lactate, only starting with 0.5mM with two subsequent of 0.5mL additions of 1M sodium lactate. A third had lactate-replete conditions (20mM) and abundant phosphate in the media (the usual M1 recipe with 4.3mM phosphate[36]).

In abiotic experiments, we added either sodium sulfide (Na_2S) or ferrous chloride ($FeCl_2$) as a titrant to the manganese(IV) oxide in the same media conditions as the biotic experiments. In the ferrous iron-induced reduction of manganese, X-ray absorption spectral parameters were adjusted to also acquire iron near-edge x-ray absorption spectra as well as the Mn edge, increasing the total spectra time to about 30 min.

Replicates of all experiments were performed either off-line, with the precipitate centrifuged and later analyzed as a sediment monolayer on tape, or in other experiments at the synchrotron under similar conditions.

RESULTS

We performed five distinct experiments with real-time measurements of manganese phase and redox state to understand the Mn reaction intermediates and products under diverse environmental conditions and reduction mechanisms. Manganese oxides are commonly reduced by sulfide, ferrous iron, and organic carbon, with the latter being a type of anaerobic respiration frequently utilized in anoxic sediments and soils[7–9]. We characterized the sequence of manganese redox state and phases which were produced during sulfide-stimulated manganese(IV) reduction, ferrous iron-induced manganese(IV) reduction, and the anaerobic respiration of manganese(IV) by the lactate-consuming bacteria *S. oneidensis.*

We observed the reduction mechanics of microbially-mediated MnO_2 reduction by lactate in three distinct experiments mimicing endmember conditions to understand processes that occur in various environments (Figure 2). We manufactured an environment with very high (4.3mM) phosphate and high (20mM) lactate to see how these might affect the intermediates and products of microbial respiration of manganese oxides. In this experiment (Figure 2a), we observed a direct transformation of MnO_2 into a Mn(II)

phosphate similar to our hureaulite [$Mn^{2+}_5(PO_3OH)_2(PO_4)_2*4H_2O$] standard (standard confirmed using Raman spectroscopy). Isosbestic points, where all spectra have the same absorbance, are only seen in two-phase conversions and these are clearly observed in the Figure 2a inset.

In contrast, the two experiments with negligible (and more realistic) phosphate have dramatically different reaction products. Our high (20mM) lactate experiment provides a reaction mechanism for what occurs when manganese oxides are limiting as compared to organic carbon concentrations, conditions which can be compared to highly productive coastal settings[47,48]. This lactate-replete experiment shows several important transitional phases with intermediates like Mn(III) oxides, Mn^{2+} in solution, and then precipitating a rhodochrosite ($MnCO_3$) product (Figure 2b). Examining the pH through time plots of each of these experiments (Figure 2a&b) demonstrates the similar beginning of both, with the consumption of MnO_2 consuming protons (Rxn 3), but then the two plots have very different secondary phases. Figure 2a shows that with high phosphate levels, the system is quickly stabilized as Mn(II)-phosphate forms and there is little subsequent change to the pH. With low phosphate levels, one can see a very different reaction progression in Figure 2b: pH continues to rise past the ~8.35 we saw in Figure 2a all the way up to ~8.6, and then pH rapidly drops followed by a slow decrease approximately back to its original pH of 8. This pH drop can be accounted for by the precipitation of $MnCO_3$:

$$Mn^{2+} + CO_2 + H_2O \rightleftharpoons MnCO_3 + 2\ H^+ \quad (4)$$

Another minimal-phosphate experiment had an additional limitation in its organic carbon (lactate) source, comparable to an oligotrophic open-ocean marine setting without many nutrients or much primary productivity producing organic carbon[47,48]. This experiment shows the production of a Mn(III) oxyhydroxide and Mn^{2+} (Figure 2c). The media began with just 0.5mL of 1M lactate, which upon addition of *S. oneidensis* was used by the bacteria to convert Mn(IV) to Mn^{2+}. This yielded approximately 11% Mn^{2+}, which we calculated by fitting the spectra to a birnessite and a Mn^{2+} standard using the Linear Fit function in Sixpack (Webb et al, 2005). We added two more aliquots of 0.5mL 1M lactate, which led to growth of a Mn(III) phase similar to what we saw as a transient phase in the high-lactate experiments. The second aliquot (dubbed t2, Figure 2c) made a stable mixture of aqueous Mn^{2+} (33%), feitknechtite [MnOOH, chosen by fitting routine over Mn_2O_3] (15%), and remnant birnessite (51%). The third aliquot (t3) temporarily made up to ~34% feitknechtite (with 26% remnant MnO_2 and 40% Mn^{2+}) but then stabilized into a system with 18% remnant birnessite, 60% Mn^{2+}, and 22% feitknechtite. Our spectral measurements indicate that this combination was stable for at least ~1 hr, but it would likely remain even longer as no redox changes could occur without addition of a reductant (Figure 2c). The development of three distinct redox equilibria can be observed in the unchanging pH plateaus (Figure 2c).

Abiotic experiments also formed a Mn(III) phase intermediate, but the Mn(II) product was highly distinct. Both sulfide (Figure 3a) and ferrous iron (Figure 3b,c) titration experiments have Mn(III) intermediates, although the sulfide spectral sequence is clearer. With sufficient reductant, however, both abiotic experiments form aqueous Mn^{2+} without any mineral product. This result is artificial in the case of sulfide-induced Mn(IV) reduction, since the increase in pH and alkalinity indicate that Mn-carbonate may have formed if enough dissolved inorganic carbon was present (an experiment for future work). In ferrous iron-induced Mn(IV) reduction, the decrease in pH indicates that this reaction should not promote carbonate precipitation but should always make Mn^{2+}, which can then be lost to the environment[19]. In these experiments, iron appears to be rapidly oxidized as it reduces Mn(IV) (Figure 3b), closely matching our FeOOH (goethite) standard and even more similar to the lepidocrocite spectra shown in O'day et al[49].

DISCUSSION

We present observations from a suite of manganese oxide reduction experiments representing diverse environmental conditions and reductants from the anaerobic respiration of Mn(IV) in soil, coastal marine, and oligotrophic ocean-like conditions to abiotic iron and sulfide titrations. There were distinct differences in each biotic experiment, where phosphate-rich conditions led to the direct formation of a Mn(II)-phosphate product, and phosphate-poor conditions formed Mn(III) oxides and eventually Mn(II)-carbonates (rhodochrosite) if given sufficient organic carbon. These all contrasted

with abiotic experiments, with both ferrous iron- and sulfide-induced reductions of Mn(IV) forming Mn(III) intermediates and then aqueous Mn^{2+}.

Each experiment we performed provides insight into how manganese(IV) oxides are reduced and how the environment impacts this reduction. If Mn(IV) is reduced abiotically, especially if the reductant is ferrous iron, then Mn^{2+} is formed and, in the environment, would likely diffuse away and not enter the sediments as potential storage of manganese (or a geologically-observable deposit of manganese). The dropping pH in the ferrous iron-induced reduction signifies that aqueous Mn^{2+} will be more and more soluble and Mn(II) hydroxide and Mn(II) carbonate phase precipitation will not be promoted (Figure 3b,c).

One exception here is the Mn(III) intermediate in both abiotic experiments (Figure 3). It appears first as an extension of the Mn(IV) peak, probably as a mixed Mn(III,IV) oxide, and later as a flattened shoulder (see t8-12 in Fig3a), but only arising after a Mn(II) shoulder is present. Because of this relative timing, we believe that this Mn(III) is forming from comproportionation reactions between produced Mn^{2+} and still-present Mn(IV) oxides, as in Reaction 4:

$$Mn^{2+} + Mn(IV)O_2 + 2\ H_2O \rightleftharpoons\ Mn(III)OOH + 2\ H^+$$

If this Mn(III) intermediate is indeed a Mn(III) oxyhydroxide precipitate, then it would retain manganese as a solid and be a stable product to potentially enter the sedimentary record, as long as there was limiting sulfide or ferrous iron (like product in Figure 3c). As we observed in other experiments, if there is a surplus of reductant, then all the manganese is converted to Mn^{2+} and, in the case of sulfide and ferrous iron, does not form a mineralogical product in our experiments.

There is a caveat in the case of the sulfide-induced reduction experiment: our data contrasts with previous work that has noted reactions between sulfide and Mn(IV) oxides producing rhodochrosite[27–30]. These other reports were all in natural sediments with active microbial cycling and respiration[28], or in experiments with microbes performing thiosulfate or sulfur disproportionation in the presence of Mn(IV) oxides[27], or with concomitant manganese oxide reduction and either sulfate or thiosulfate reduction[29,30]. All of these circumstances would have high dissolved inorganic carbon, as well as elevated alkalinity, and these conditions would promote the precipitation of carbonates including rhodochrosite. We note that our experiments began with essentially no dissolved inorganic carbon, and so even though we measured increasing pHs in our sulfide-induced manganese reduction experiment, no Mn(II)-carbonate could form. Exploring how much dissolved inorganic carbon is required for rhodochrosite precipitation associated with sulfide-MnO_2 reactions is beyond the scope of this project, but should be investigated in further work.

Kinetic Controls on Microbially-Mediated Reaction Sequences The microbial reduction of Mn(IV) oxides also shows a Mn(III) oxyhydroxide secondary phase, but only when phosphate is deficient. This observation yields important insights into the kinetics of Mn-phosphates and Mn-carbonates: Mn-phosphates must form significantly more rapidly than Mn-carbonates. This inference is supported by what is known about these two minerals, where Mn-phosphates have been observed to dominate over rhodochrosite in a phosphate-rich meromictic lake (Hongve, 1997) and experiments that show rhodochrosite has even slower precipitation rates than calcite[50,51]. We clearly see in the high-phosphate experiments that there is a two-phase system: directly after Mn(II) is produced, Mn(II)-phosphate is precipitated because we don't see any aqueous Mn^{2+} build up in solution and contribute to the spectra (Figure 2a). The lack of Mn(III) oxyhydroxide in the phosphate-rich experiments reveals the speedy precipitation kinetics of Mn(II)-phosphate, and also indicates that *S. oneidensis* produces Mn^{2+} directly (or at least in two very rapid one-electron transfers) as we cannot resolve a Mn(III) step in the high-phosphate experiments (Figure 4). Some studies have shown a Mn(III) step during the reduction of Mn(IV)[38], but this is likely a very fast intermediate, and may have been promoted by their experimental conditions (with the high concentrations of pyrophosphate).

The major differences between the phosphate and low-phosphate experiments can be solely explained by a combination of precipitation kinetics and environmental controls (Figure 4). Our low-phosphate experiments show a Mn(II) shoulder grow while Mn(IV)

oxides become more and more enriched in Mn(III), much more similar to the abiotic reduction experiments (Figure 2b,c). This Mn(III) phase with varying amounts of Mn(IV) and Mn^{2+} can be stabilized if more organic carbon is not added, as we show in our lactate-limiting experiment (Figure 2c). With lactate-replete conditions, this trend continues until aqueous Mn^{2+} dominates the entire system. Then slowly, the Mn(II) peak position shifts and the 6563 second peak of rhodochrosite forms and the system transitions to being completely Mn-carbonate (Figure 2b). The formation of Mn(III) oxyhydroxides, suggesting that there is sufficient Mn^{2+} accumulation to react with Mn(IV) oxides, and the long presence of aqueous Mn^{2+} (>1.5 hrs), indicate that the formation of Mn(II)-carbonate is highly kinetically-impaired as expected (Figure 4). The lack of Mn^{2+} in the high-phosphate experiments establishes that the kinetics of Mn(II)-phosphate precipitation is much faster than Mn^{2+} generation, Mn(III)OOH formation, or Mn(II)-carbonate precipitation in general (Figure 4). The build-up of aqueous Mn^{2+} in the low-phosphate experiments reveals that the kinetics of Mn(IV) reduction must also be faster than rhodochrosite precipitation (Figure 4). The rate of Mn(III) oxyhydroxide formation seems to be be faster than the reduction of that Mn(III) phase by *S. oneidensis* since we do see this phase spectrally (although not for very long), but Mn(III) oxyhydroxide formation must be slower than Mn(II)-phosphate precipitation as we do not see it appear in the phosphate-replete experiments (Figure 4).

Our diverse manganese reduction experiments not only yield insights into the kinetic controls on intermediates (which can be products with incomplete reactions), but we also

present preliminary evidence that reaction products can potentially be diagnostic for reaction pathway and environmental conditions. Mn(II)-phosphates only formed when there were very high (mM) concentrations of phosphate in the media. Mn(II)-carbonates (rhodochrosite) precipitated with high lactate and limiting phosphate, suggesting that this mineral should form in similar natural conditions when organic carbon is in excess of Mn(IV) oxides. In simple systems free of dissolved inorganic carbon, sulfide- and ferrous iron-induced reduction of Mn(IV) oxides produced only soluble Mn^{2+}, but further experiments are necessary to examine whether Mn(II)-carbonates can form abiotically under more realistic conditions with inorganic carbon present. When Mn^{2+} is formed, this soluble product will be able to migrate away from the reaction locus. If surrounding conditions are anoxic, this could result in a Mn loss to the system. If these reactions are occurring in sediments near the oxic-anoxic boundary, then this may simply recycle Mn back to where there is oxygen and Mn^{2+} can be re-oxidized and re-precipitated.

Mn(III) oxyhydroxides are intriguing yet complex: they appear to form in both abiotic and biotic reduction reactions, and thus are not distinctive for reduction pathway, but they also present as an appealing precursor to the Mn(III) phase in the rock record, braunite. One of the proposed pathways of braunite formation involves reacting a Mn(III) oxide, Mn_2O_3, with silica (SiO_2)[52], and this Mn(III) oxyhydroxide may be an attractive phase to begin this reaction with. In the rock record, braunite is always present with Mn(II)-carbonates (Johnson et al, Chapter 1), which, according to our experiments, is consistent with microbial Mn(IV) reduction since that reaction does make a Mn(III) oxyhydroxide

and (eventually) Mn(II)-carbonate and the reaction extent could be separated in pore spaces to have access to different levels of organic carbon. A mixture of Mn(III) oxides and Mn(II) carbonate could also be formed in any system with manganese oxides, a reductant that does not lower the pH (i.e., not ferrous iron), and sufficient dissolved inorganic carbon, so this assemblage does not necessarily imply a microbial presence.

Time-resolved measurements throughout the reduction sequences of microbial manganese oxide reduction harnessing lactate and abiotic manganese oxide reduction with sulfide and ferrous iron reveal the importance of kinetics and geochemical environment to understand reaction pathways and products. We observe $MnCO_3$ (rhodochrosite) precipitation upon microbial MnO_2 reduction with deficient phosphate and high organic carbon conditions, but a Mn(II)-phosphate product when phosphate is abundant. The kinetics of Mn(II)-phosphate precipitation are so rapid that the high-phosphate experiments show that Mn(IV) reduction by *S. oneidensis* is effectively a 2-electron reduction. Mn(III) oxyhydroxides are formed during other reduction conditions, and reductant availability predominantly controls whether Mn(III) oxyhydroxides are formed as an intermediate or a product. Abiotic MnO_2 reduction using ferrous iron and sulfide terminally produced Mn^{2+} in solution, but MnO_2-sulfide reactions could produce $MnCO_3$ with available dissolved inorganic carbon. By recognizing unique products from different MnO_2 reduction pathways, we can now begin to more accurately link the geologic record on Earth with a process-based understanding of mineral genesis.

ACKNOWLEDGEMENTS

We would like to express our gratitude to Cynthia Patty, John Bargar, Courtney Roach, and Cathy Knotts for going above and beyond so that it was possible for us to run these experiments at the synchrotron; to Jeffrey Gralnick, Annie Rowe and Jim Hemp for experimental assistance and advice; and to George Rossman for assistance and frequent access to his RAMAN and Fourier Transform Infrared Spectrometer. We acknowledge a Packard Foundation grant to W.W.F., which funded much of this research, and an NSF Graduate Research Fellowship to J.E.J. Portions of this research were carried out at the Stanford Synchrotron Radiation Lightsource, a Directorate of SLAC National Accelerator Laboratory and an Office of Science User Facility operated for the US Department of Energy Office of Science by Stanford University.

FIGURES

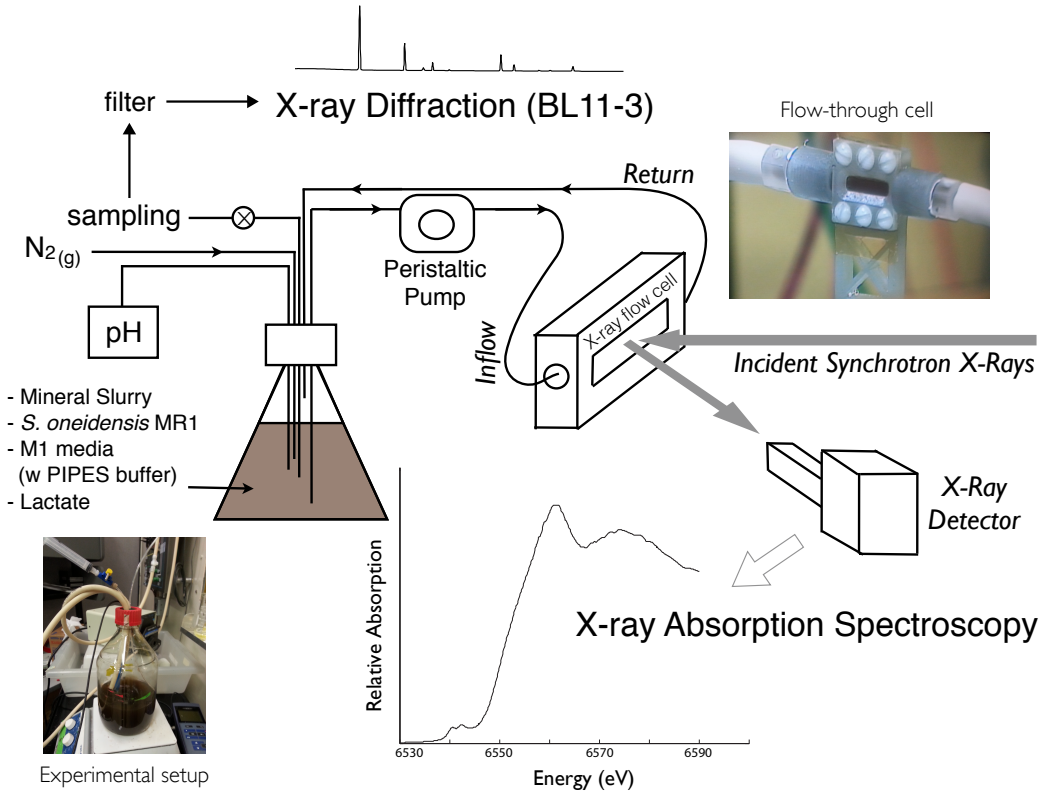

Figure 1 – Schematic of flow-through system showing reaction vessel with colloidal manganese oxide mineral slurry, M1 media with PIPES buffer, and (depending on experiment) lactate and *S. oneidensis.* The reaction vessel was kept anoxic with N_2 and pH was measured via an environmental pH probe. A sampling portal enabled acquisition of hourly filter samples to be later measured on a synchrotron X-ray diffraction beam line. A peristaltic pump brought a representative portion of the flow-through cell through anaerobic tubing into the beam line hutch, where the X-ray beam could sample the Mn mineralogy, coordination environment and redox state through a window on an X-ray flow through cell. The resultant X-ray absorption spectra was measured on a X-ray detector. Photos of the reaction vessel and flow-through cell are shown alongside the schematic drawing.

Figure 2

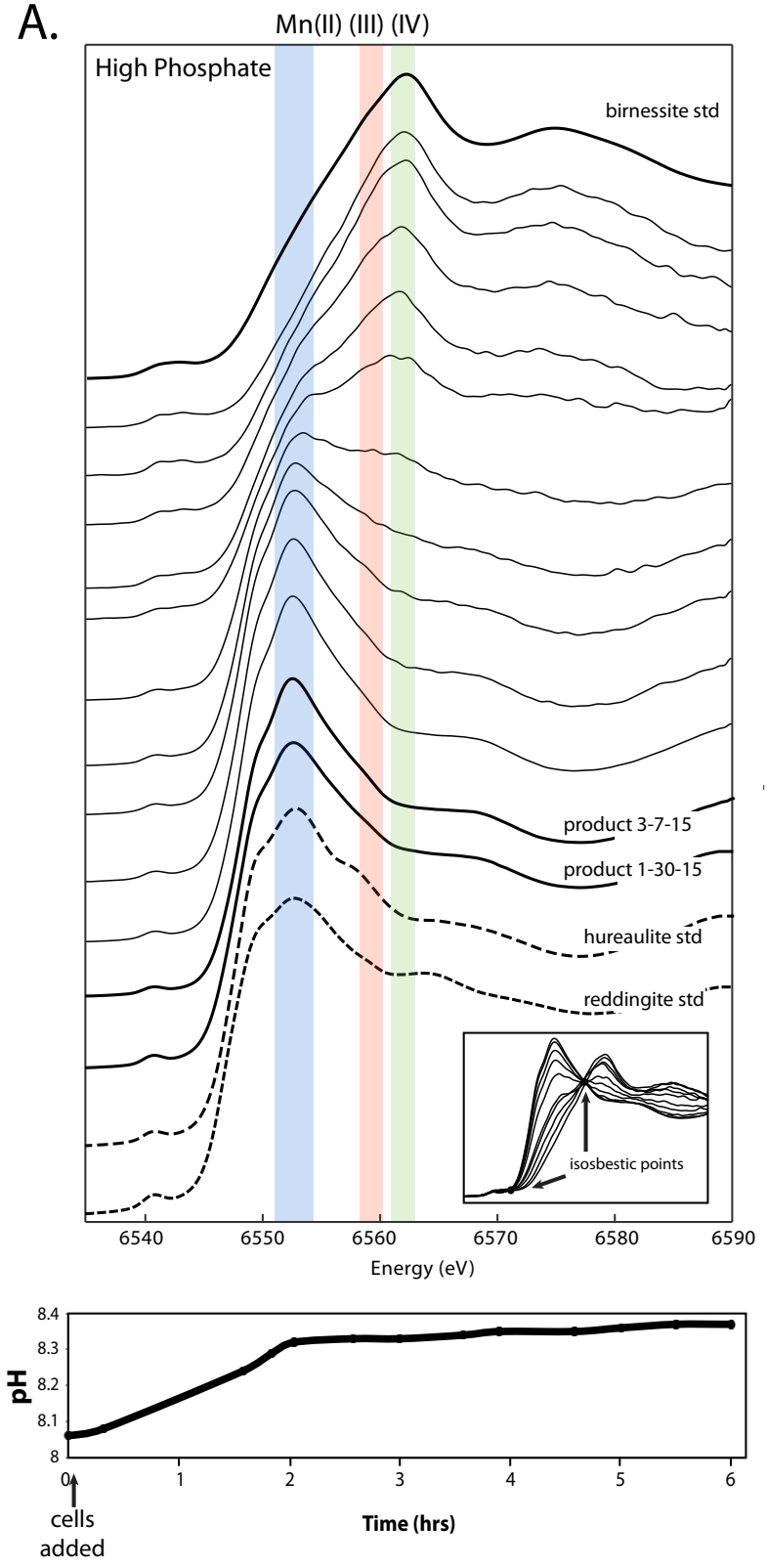
A.
Mn(II) (III) (IV)
High Phosphate
birnessite std
product 3-7-15
product 1-30-15
hureaulite std
reddingite std
isosbestic points
6540
6550
6560
6570
6580
6590
Energy (eV)
pH
8.4
8.3
8.2
8.1
8
0
1
2
3
4
5
6
cells added
Time (hrs)

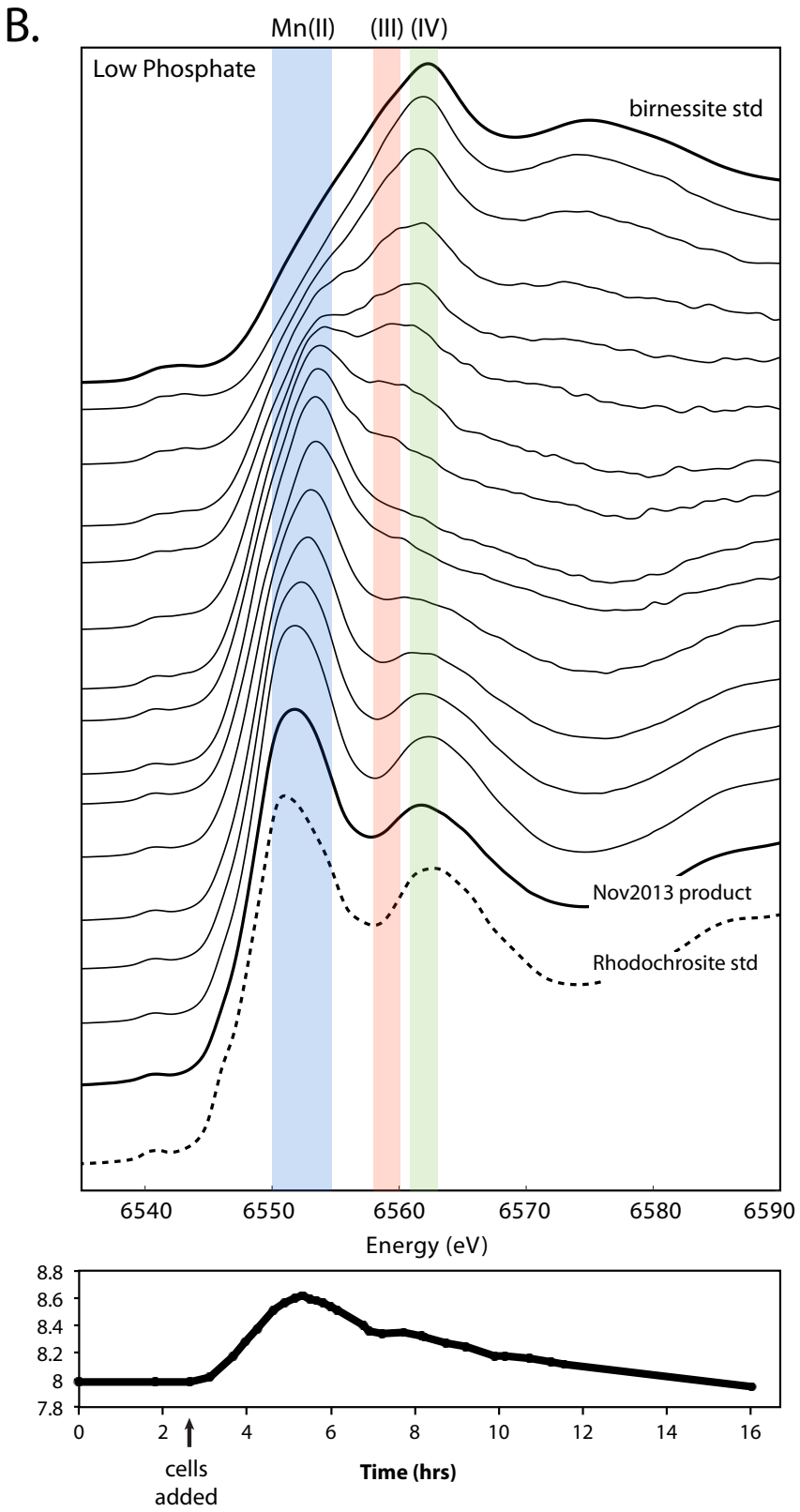
B.
Mn(II)
(III) (IV)
Low Phosphate
birnessite std
Nov2013 product
Rhodochrosite std
6540
6550
6560
6570
6580
6590
Energy (eV)
8.8
8.6
8.4
8.2
8
7.8
0
2
4
6
8
10
12
14
16
cells
added
Time (hrs)

C.

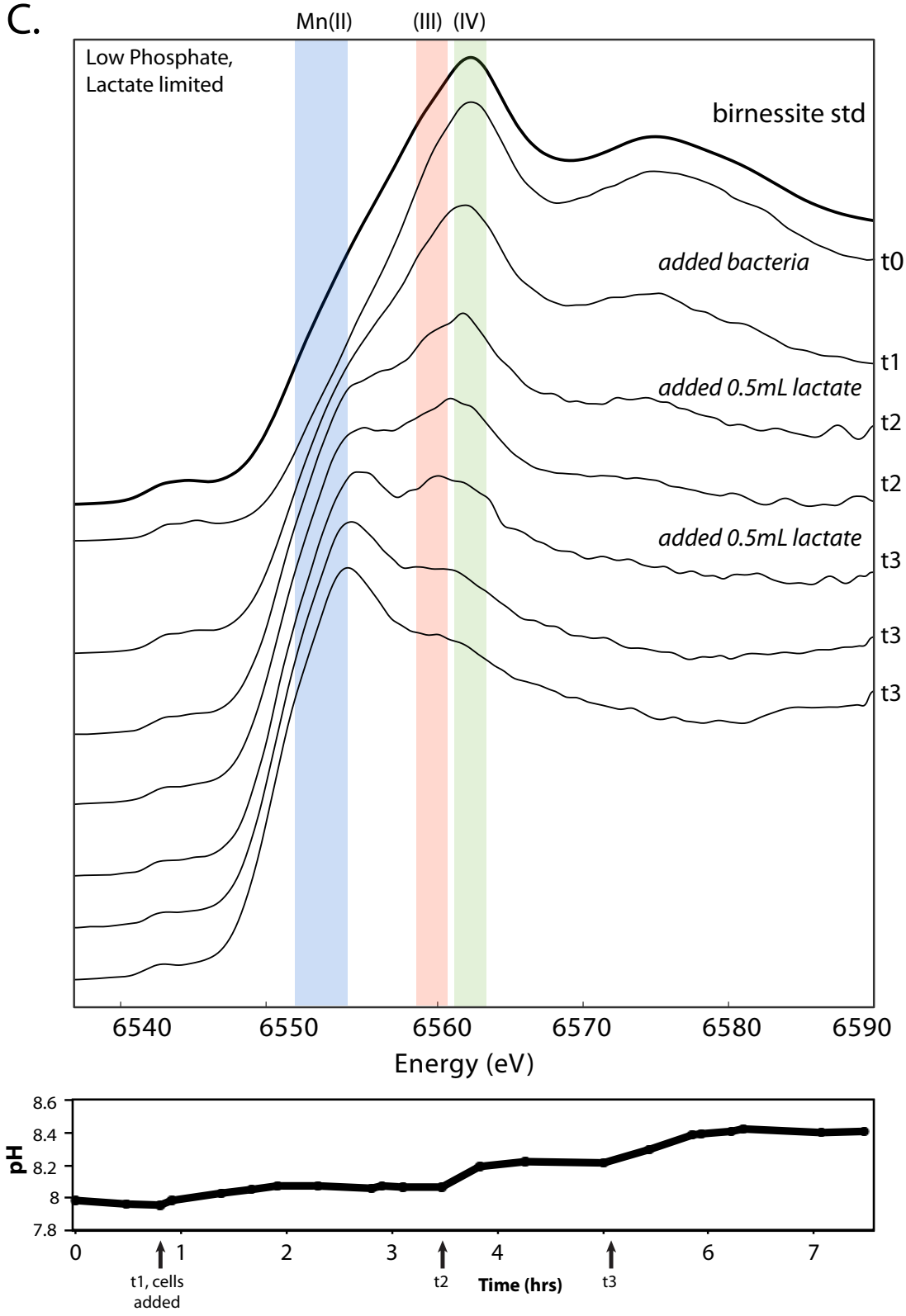
Mn(II)
(III)
(IV)
Low Phosphate,
Lactate limited
birnessite std
added bacteria
t0
t1
added 0.5mL lactate
t2
t2
added 0.5mL lactate
t3
t3
t3
6540
6550
6560
6570
6580
6590
Energy (eV)
pH
8.6
8.4
8.2
8
7.8
0
1
2
3
4
6
7
t1, cells
added
t2
Time (hrs)
t3

Figure 2 – Three representative microbial reduction experiments observing the reduction sequence induced by *S. oneidensis* are depicted via a waterfall, with the initial colloidal MnO_2 (MnIV, similar to a birnessite) at the top and the progression of spectra shown descending to a final product at the bottom. When appropriate, relevant standard spectra are shown below the product spectra. A time course of pH measurements is plotted below each experiment. A. High (4.3mM) phosphate experiment, proceeding from MnO_2 to a Mn(II) phosphate similar to hureaulite ($Mn^{2+}_5(PO_3OH)_2(PO_4)_2*4H_2O$). B. High (20mM) lactate experiment, evolving colloidal MnO_2 to rhodochrosite ($MnCO_3$). A product from an earlier experiment and a rhodochrosite standard are shown for comparison. C. Lactate-limited experiment, beginning at 0.5mM lactate with two additions of 0.5mM lactate. See text for further details.

Figure 3 (below) – Three representative abiotic reduction experiments observing the reduction sequence induced by various species are depicted via a waterfall, with the initial colloidal MnO_2 (similar to a MnIV birnessite) at the top and the progression of spectra shown descending to a final product at the bottom. When appropriate, relevant standard spectra are shown below the product spectra. pH measurements are plotted below each experiment. A. Sulfide-induced manganese oxide reduction, evolving to a Mn^{2+} solution. B. Ferrous iron titration of manganese oxides, with both manganese and iron X-ray absorption spectra shown. Mn(IV) proceeds to Mn^{2+} while iron added all appears to be rapidly oxidized to Fe(III) oxides. pH drops with each iron addition. C. Another representative experiment showing how ferrous iron reduces manganese. Only manganese spectra are shown. This is an incomplete reduction and a Mn(III) phase can be observed.

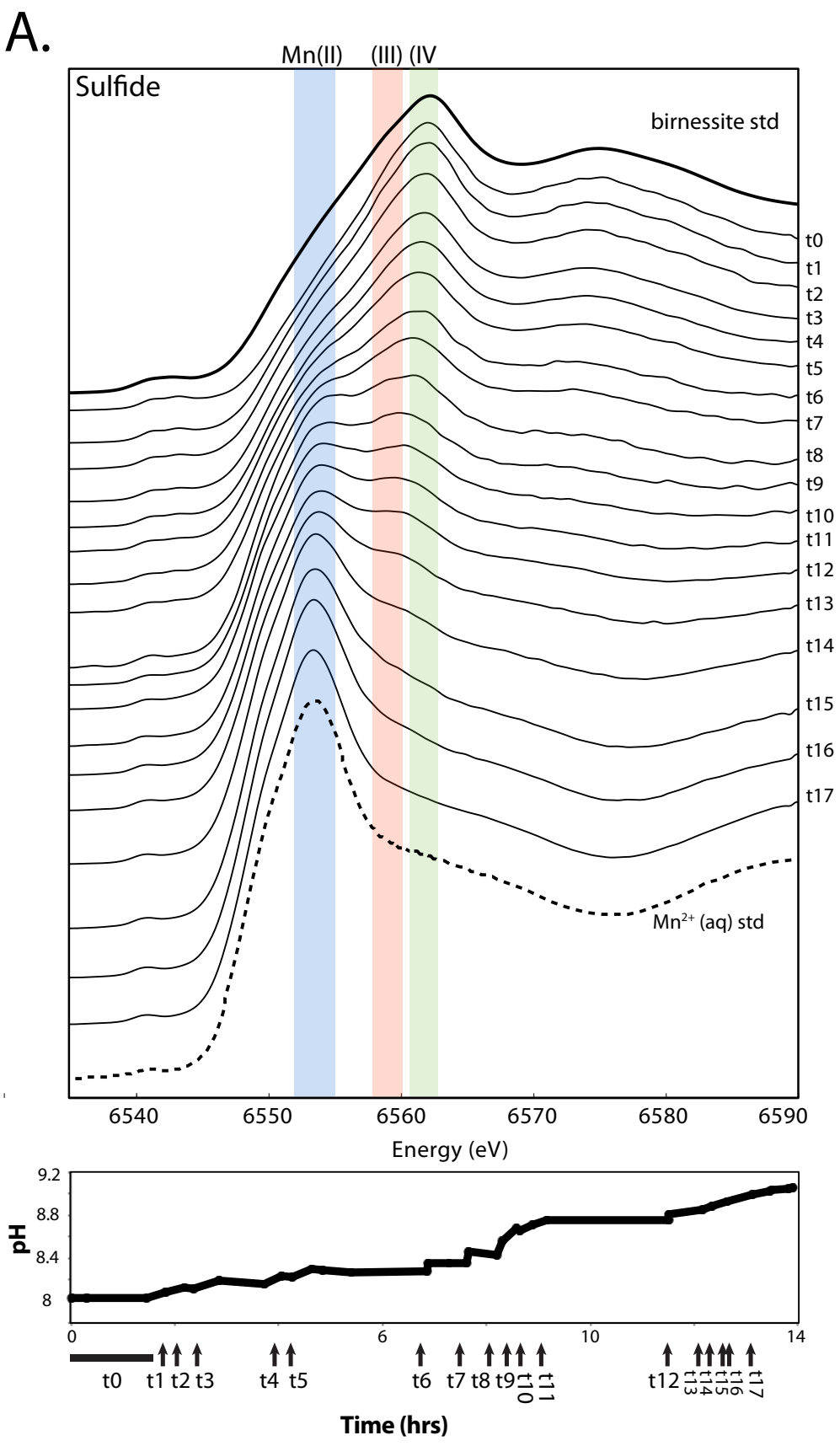
A.
Mn(II)
(III)
(IV
Sulfide
birnessite std
t0
t1
t2
t3
t4
t5
t6
t7
t8
t9
t10
t11
t12
t13
t14
t15
t16
t17
Mn2+ (aq) std
6540
6550
6560
6570
6580
6590
Energy (eV)
9.2
8.8
8.4
8
pH
0
6
10
14
t0
t1 t2 t3
t4 t5
t6
t7 t8 t9
t10
t11
t12
t13
t14
t15
t16
t17
Time (hrs)

B.

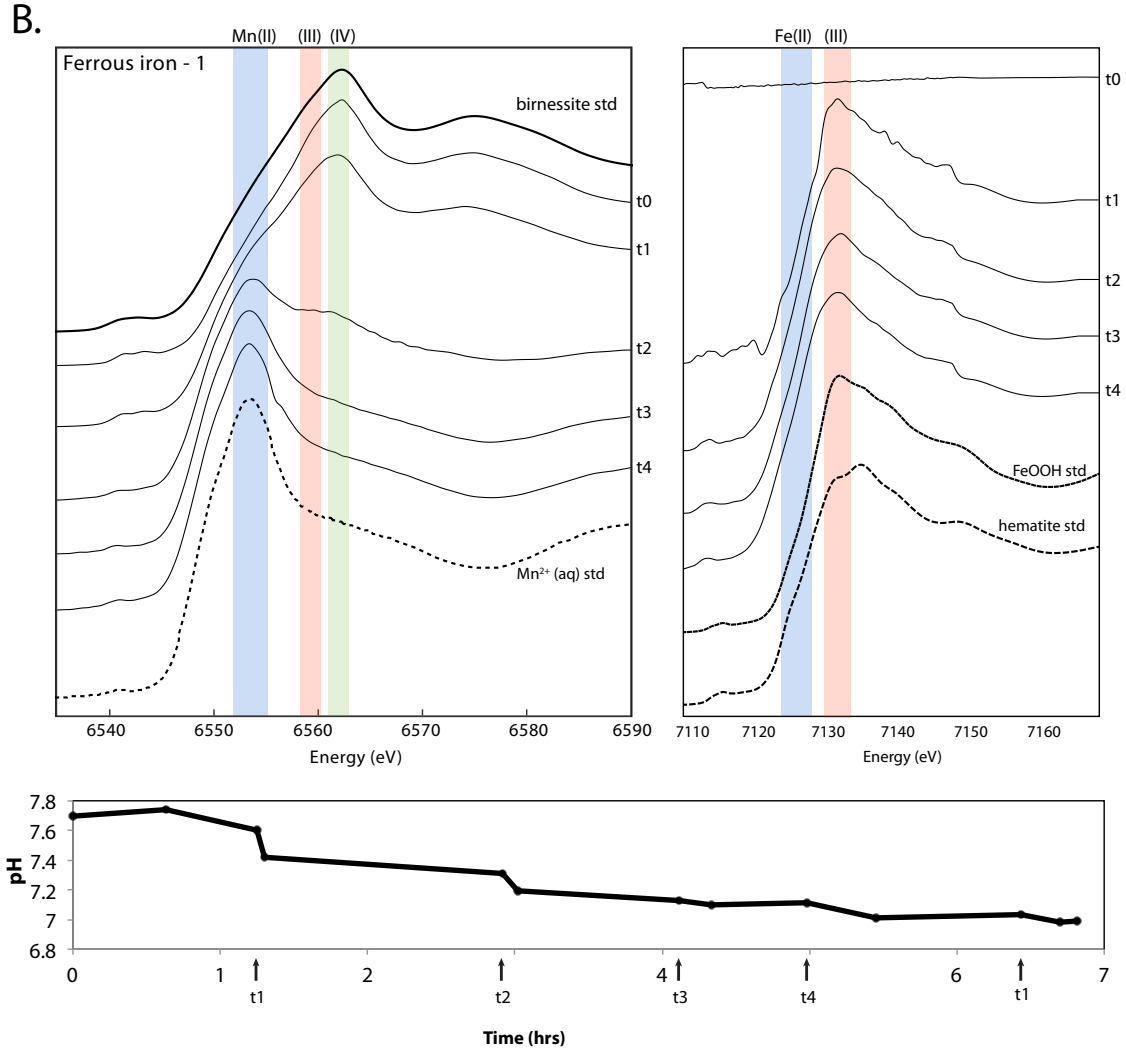
Ferrous iron - 1
Mn(II)
(III)
(IV)
birnessite std
t0
t1
t2
t3
t4
Mn2+ (aq) std
6540
6550
6560
6570
6580
6590
Energy (eV)
Fe(II)
(III)
t0
t1
t2
t3
t4
FeOOH std
hematite std
7110
7120
7130
7140
7150
7160
Energy (eV)
pH
7.8
7.6
7.4
7.2
7
6.8
0
1
2
4
6
7
t1
t2
t3
t4
t1
Time (hrs)

C.

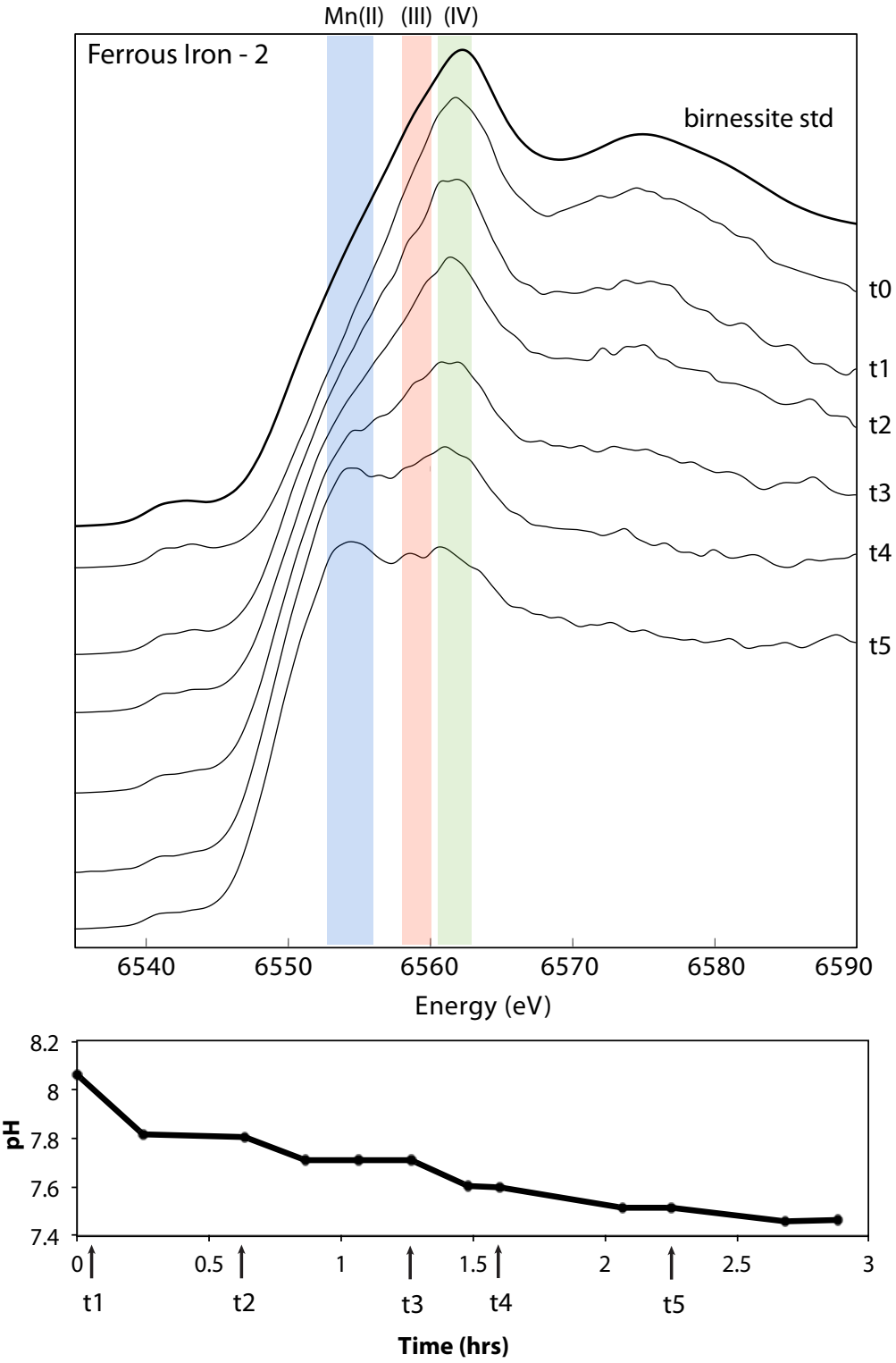
Mn(II) (III) (IV)
Ferrous Iron - 2
birnessite std
t0
t1
t2
t3
t4
t5
6540
6550
6560
6570
6580
6590
Energy (eV)
8.2
8
7.8
7.6
7.4
pH
0
0.5
1
1.5
2
2.5
3
t1
t2
t3
t4
t5
Time (hrs)

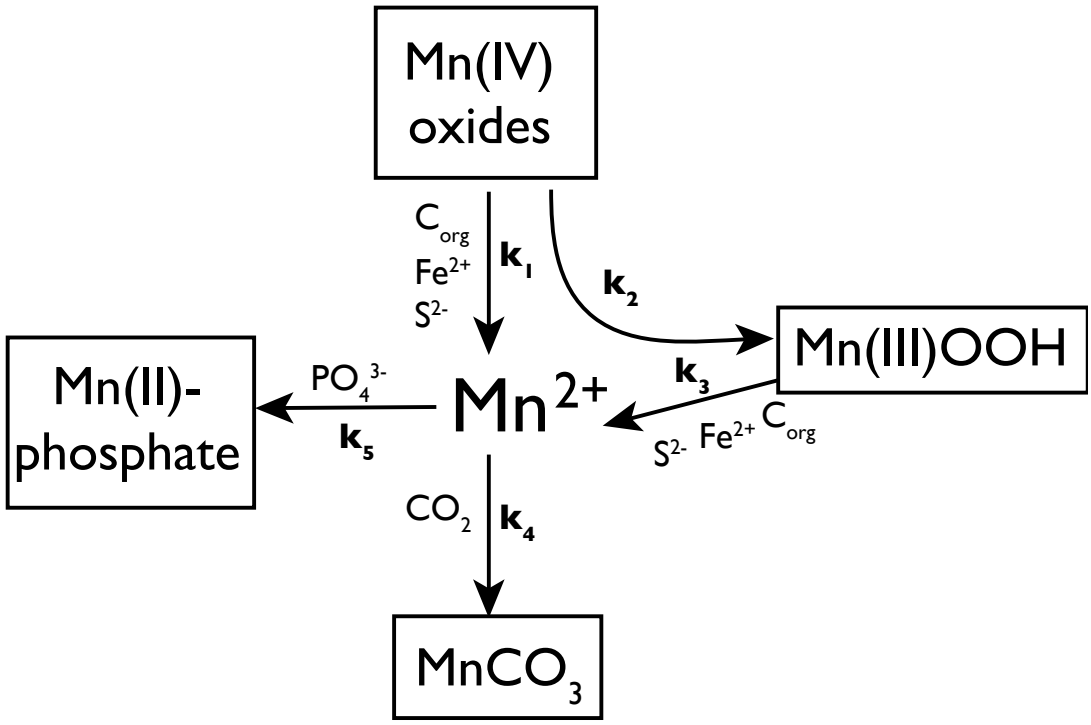

Figure 4 – Our model of how various manganese reduction pathways lead to Mn^{2+}, which then can react with Mn(IV) oxides to produce Mn(III) oxyhydroxides or precipitate as Mn(II) phosphates or Mn(II)CO_3.

k_1: kinetic rate constant for reduction of Mn(IV) to Mn^{2+}

k_2: kinetic rate constant for comproportionation reaction between Mn(IV) and Mn^{2+} to Mn(III) oxyhydroxides

k_3: kinetic rate constant for reduction of Mn(III) to Mn^{2+}

k_4: kinetic rate constant for precipitation of $MnCO_3$ from Mn^{2+} and CO_3^{2-}

k_5: kinetic rate constant for precipitation of $MnCO_3$ from Mn^{2+} and PO_4^{3-}

REFERENCES

(1) Tebo, B. M.; Johnson, H. A.; McCarthy, J. K.; Templeton, A. S. Geomicrobiology of manganese(II) oxidation. *Trends Microbiol.* **2005**, *13* (9), 421–428.

(2) Post, J. E. Manganese oxide minerals: Crystal structures and economic and environmental significance. *Proc. Natl. Acad. Sci.* **1999**, *96* (7), 3447–3454.

(3) Calvert, S. E.; Pedersen, T. F. Sedimentary geochemistry of manganese; implications for the environment of formation of manganiferous black shales. *Econ. Geol.* **1996**, *91* (1), 36–47.

(4) Armstrong, F. A. Why Did Nature Choose Manganese to Make Oxygen? *Philos. Trans. R. Soc. B Biol. Sci.* **2008**, *363* (1494), 1263–1270.

(5) Lovley, D. R.; Phillips, E. J. P. Novel Mode of Microbial Energy Metabolism: Organic Carbon Oxidation Coupled to Dissimilatory Reduction of Iron or Manganese. *Appl. Environ. Microbiol.* **1988**, *54* (6), 1472–1480.

(6) Myers, C. R.; Nealson, K. H. Bacterial manganese reduction and growth with manganese oxide as the sole electron acceptor. *Science* **1988**, *240* (4857), 1319–1321.

(7) Van Cappellen, P.; Viollier, E.; Roychoudhury, A.; Clark, L.; Ingali, E.; Lowe, K.; Dichistrina, T. Cycling of iron and manganese in surface sediments; a general theory for the coupled transport and reaction of carbon, oxygen, nitrogen, sulfur, iron, and manganese. *Environ. Sci. Technol.* **1998**, *32*, 2931–2939.

(8) Canfield, D. E.; Thamdrup, B.; Hansen, J. W. The anaerobic degradation of organic matter in Danish coastal sediments: Iron reduction, manganese reduction, and sulfate reduction. *Geochim. Cosmochim. Acta* **1993**, *57* (16), 3867–3883.

(9) Thamdrup, B.; Rosselló-Mora, R.; Amann, R. Microbial Manganese and Sulfate Reduction in Black Sea Shelf Sediments. *Appl. Environ. Microbiol.* **2000**, *66* (7), 2888–2897.

(10) Burdige, D. J.; Nealson, K. H. Chemical and microbiological studies of sulfide-mediated manganese reduction. *Geomicrobiol. J.* **1986**, *4* (4), 361–387.

(11) Myers, C. R.; Nealson, K. H. Microbial reduction of manganese oxides: Interactions with iron and sulfur. *Geochim. Cosmochim. Acta* **1988**, *52* (11), 2727–2732.

(12) Ying, S. C.; Kocar, B. D.; Griffis, S. D.; Fendorf, S. Competitive Microbially and Mn Oxide Mediated Redox Processes Controlling Arsenic Speciation and Partitioning. *Environ. Sci. Technol.* **2011**, *45* (13), 5572–5579.

(13) Fredrickson, J. K.; Zachara, J. M.; Kennedy, D. W.; Liu, C.; Duff, M. C.; Hunter, D. B.; Dohnalkova, A. Influence of Mn oxides on the reduction of uranium(VI) by the metal-reducing bacterium Shewanella putrefaciens. *Geochim. Cosmochim. Acta* **2002**, *66* (18), 3247–3262.

(14) Webb, S. M.; Tebo, B. M.; Bargar, J. R. Structural characterization of biogenic Mn oxides produced in seawater by the marine bacillus sp. strain SG-1. *Am. Mineral.* **2005**, *90* (8-9), 1342–1357.

(15) Bargar, J. R.; Tebo, B. M.; Villinski, J. E. In situ characterization of Mn(II) oxidation by spores of the marine Bacillus sp. strain SG-1. *Geochim. Cosmochim. Acta* **2000**, *64*, 2775–2778.
(16) Murray, J. W.; Dillard, J. G.; Giovanoli, R.; Moers, H.; Stumm, W. Oxidation of Mn(II): Initial mineralogy, oxidation state and ageing. *Geochim. Cosmochim. Acta* **1985**, *49* (2), 463–470.
(17) Wehrli, B.; Friedl, G.; Manceau, A. Reaction Rates and Products of Manganese Oxidation at the Sediment-Water Interface. In *Aquatic Chemistry*; Advances in Chemistry; American Chemical Society, 1995; Vol. 244, pp 111–134.
(18) McKeown, D. A.; Post, J. E. Characterization of manganese oxide mineralogy in rock varnish and dendrites using X-ray absorption spectroscopy. *Am. Mineral.* **2001**, *86* (5-6), 701–713.
(19) Tebo, B. M.; Bargar, J. R.; Clement, B. G.; Dick, G. J.; Murray, K. J.; Parker, D.; Verity, R.; Webb, S. M. BIOGENIC MANGANESE OXIDES: Properties and Mechanisms of Formation. *Annu. Rev. Earth Planet. Sci.* **2004**, *32* (1), 287–328.
(20) Roy, S. Sedimentary manganese metallogenesis in response to the evolution of the Earth system. *Earth-Sci. Rev.* **2006**, *77* (4), 273–305.
(21) Maynard, J. B. The Chemistry of Manganese Ores through Time: A Signal of Increasing Diversity of Earth-Surface Environments. *Econ. Geol.* **2010**, *105* (3), 535–552.
(22) Okita, P. M.; Maynard, J. B.; Spiker, E. C.; Force, E. R. Isotopic evidence for organic matter oxidation by manganese reduction in the formation of stratiform manganese carbonate ore. *Geochim. Cosmochim. Acta* **1988**, *52* (11), 2679–2685.
(23) Johnson, J. E.; Webb, S. M.; Ma, C.; Fischer, W. W. Manganese mineralogy and diagenesis in the sedimentary rock record. *Geochim. Cosmochim. Acta* **in review**.
(24) Coleman, M. L.; Fleet, A.; Donson, P. *Preliminary studies of manganese-rich carbonate nodules from Leg 68, Site 503, eastern equatorial Pacific*; Init. Repts. DSDP 68; 1982; pp 481–489.
(25) Johnson, J. E.; Webb, S. M.; Thomas, K.; Ono, S.; Kirschvink, J. L.; Fischer, W. W. Manganese-oxidizing photosynthesis before the rise of cyanobacteria. *Proc. Natl. Acad. Sci.* **2013**, *110* (28), 11238–11243.
(26) Nealson, K. H.; Saffarini, D. Iron and Manganese in Anaerobic Respiration: Environmental Significance, Physiology, and Regulation. *Annu. Rev. Microbiol.* **1994**, *48* (1), 311–343.
(27) Böttcher, M. E.; Thamdrup, B. Anaerobic sulfide oxidation and stable isotope fractionation associated with bacterial sulfur disproportionation in the presence of MnO2. *Geochim. Cosmochim. Acta* **2001**, *65* (10), 1573–1581.
(28) Meister, P.; Bernasconi, S. M.; Aiello, I. W.; Vasconcelos, C.; Mckenzie, J. A. Depth and controls of Ca-rhodochrosite precipitation in bioturbated sediments of the Eastern Equatorial Pacific, ODP Leg 201, Site 1226 and DSDP Leg 68, Site 503. *Sedimentology* **2009**, *56* (5), 1552–1568.
(29) Huckriede, H.; Meischner, D. Origin and environment of manganese-rich sediments within black-shale basins. *Geochim. Cosmochim. Acta* **1996**, *60* (8), 1399–1413.

(30) Lee, J.-H.; Kennedy, D. W.; Dohnalkova, A.; Moore, D. A.; Nachimuthu, P.; Reed, S. B.; Fredrickson, J. K. Manganese sulfide formation via concomitant microbial manganese oxide and thiosulfate reduction. *Environ. Microbiol.* **2011**, *13* (12), 3275–3288.
(31) Fischer, T. B.; Heaney, P. J.; Jang, J.-H.; Ross, D. E.; Brantley, S. L.; Post, J. E.; Tien, M. Continuous time-resolved X-ray diffraction of the biocatalyzed reduction of Mn oxide. *Am. Mineral.* **2008**, *93* (11-12), 1929–1932.
(32) Brown, G. E.; Sturchio, N. C. An Overview of Synchrotron Radiation Applications to Low Temperature Geochemistry and Environmental Science. *Rev. Mineral. Geochem.* **2002**, *49* (1), 1–115.
(33) Manceau, A.; Marcus, M. A.; Grangeon, S. Determination of Mn valence states in mixed-valent manganates by XANES spectroscopy. *Am. Mineral.* **2012**, *97*, 816–827.
(34) Bargar, J. R.; Webb, S. M.; Synchrotron, S. Structural Determination of Marine Bacteriogenic Manganese Oxides oxides. *Sci. York* **2005**, No. August, 1–4.
(35) Webb, S. M.; Dick, G. J.; Bargar, J. R.; Tebo, B. M. Evidence for the presence of Mn(III) intermediates in the bacterial oxidation of Mn(II). *Proc. Natl. Acad. Sci. U. S. A.* **2005**, *102* (15), 5558–5563.
(36) Kostka, J.; Nealson, K. H. Isolation, Cultivation and Characterization of Iron- and Manganese-Reducing Bacteria. In *Techniques in Microbial Ecology*; Burlage, R. S., Atlas, R., Stahl, D., Geesey, G., Sayler, G., Eds.; Oxford University Press: Oxford, 1998; p 468.
(37) Richardson, D. J.; Butt, J. N.; Fredrickson, J. K.; Zachara, J. M.; Shi, L.; Edwards, M. J.; White, G.; Baiden, N.; Gates, A. J.; Marritt, S. J.; et al. The "porin-cytochrome" model for microbe-to-mineral electron transfer. *Mol. Microbiol.* **2012**, *85* (2), 201–212.
(38) Lin, H.; Szeinbaum, N. H.; DiChristina, T. J.; Taillefert, M. Microbial Mn(IV) reduction requires an initial one-electron reductive solubilization step. *Geochim. Cosmochim. Acta* **2012**, *99*, 179–192.
(39) Harris, H. W.; El-Naggar, M. Y.; Bretschger, O.; Ward, M. J.; Romine, M. F.; Obraztsova, A. Y.; Nealson, K. H. Electrokinesis is a microbial behavior that requires extracellular electron transport. *Proc. Natl. Acad. Sci.* **2010**, *107* (1), 326–331.
(40) Marsili, E.; Baron, D. B.; Shikhare, I. D.; Coursolle, D.; Gralnick, J. A.; Bond, D. R. Shewanella secretes flavins that mediate extracellular electron transfer. *Proc. Natl. Acad. Sci.* **2008**, *105* (10), 3968–3973.
(41) Kotloski, N. J.; Gralnick, J. A. Flavin electron shuttles dominate extracellular electron transfer by Shewanella oneidensis. *mBio* **2013**, *4* (1).
(42) Gorby, Y. A.; Yanina, S.; McLean, J. S.; Rosso, K. M.; Moyles, D.; Dohnalkova, A.; Beveridge, T. J.; Chang, I. S.; Kim, B. H.; Kim, K. S.; et al. Electrically conductive bacterial nanowires produced by Shewanella oneidensis strain MR-1 and other microorganisms. *Proc. Natl. Acad. Sci.* **2006**, *103* (30), 11358–11363.

(43) Myers, C. R.; Myers, J. M. Localization of cytochromes to the outer membrane of anaerobically grown Shewanella putrefaciens MR-1. *J. Bacteriol.* **1992**, *174* (11), 3429–3438.
(44) Okamoto, A.; Hashimoto, K.; Nealson, K. H.; Nakamura, R. Rate enhancement of bacterial extracellular electron transport involves bound flavin semiquinones. *Proc. Natl. Acad. Sci. U. S. A.* **2013**, *110* (19), 7856–7861.
(45) Bergmann, K. D.; Grotzinger, J. P.; Fischer, W. W. Biological Influences on Seafloor Carbonate Precipitation. *PALAIOS* **2013**, *28* (2), 99–115.
(46) Conkright, M. E.; Garcia, H. E.; O'Brien, T. D.; Locarnini, R. A.; Boyer, T. P.; Antonov, C. S. *World Ocean Atlas 2001*; Levitus, E., Ed.; NOAA Atlas NESDIS 52; U.S. Gov. Printing Office: Wash., D.C., 2002; Vol. 4: Nutrients.
(47) Williams, R. G.; Follows, M. J. *Ocean Dynamics and the Carbon Cycle: Principles and Mechansims*; Cambridge University Press: New York City, 2011.
(48) O'Day, P. A.; Rivera, N.; Root, R.; Carroll, S. A. X-ray absorption spectroscopic study of Fe reference compounds for the analysis of natural sediments. *Am. Mineral.* **2004**, *89* (4), 572–585.
(49) Sternbeck, J. Kinetics of rhodochrosite crystal growth at 25°C: The role of surface speciation. *Geochim. Cosmochim. Acta* **1997**, *61* (4), 785–793.
(50) Jensen, D. L.; Boddum, J. K.; Tjell, J. C.; Christensen, T. H. The solubility of rhodochrosite (MnCO3) and siderite (FeCO3) in anaerobic aquatic environments. *Appl. Geochem.* **2002**, *17* (4), 503–511.
(51) Robie, R. A.; Huebner, J. S.; Hemingway, B. S. Heat capacities and thermodynamic properties of braunite (Mn7SiO12) and rhodonite (MnSiO3). *Am. Mineral.* **1995**, *80*, 560–575.

SUPPORTING FIGURES

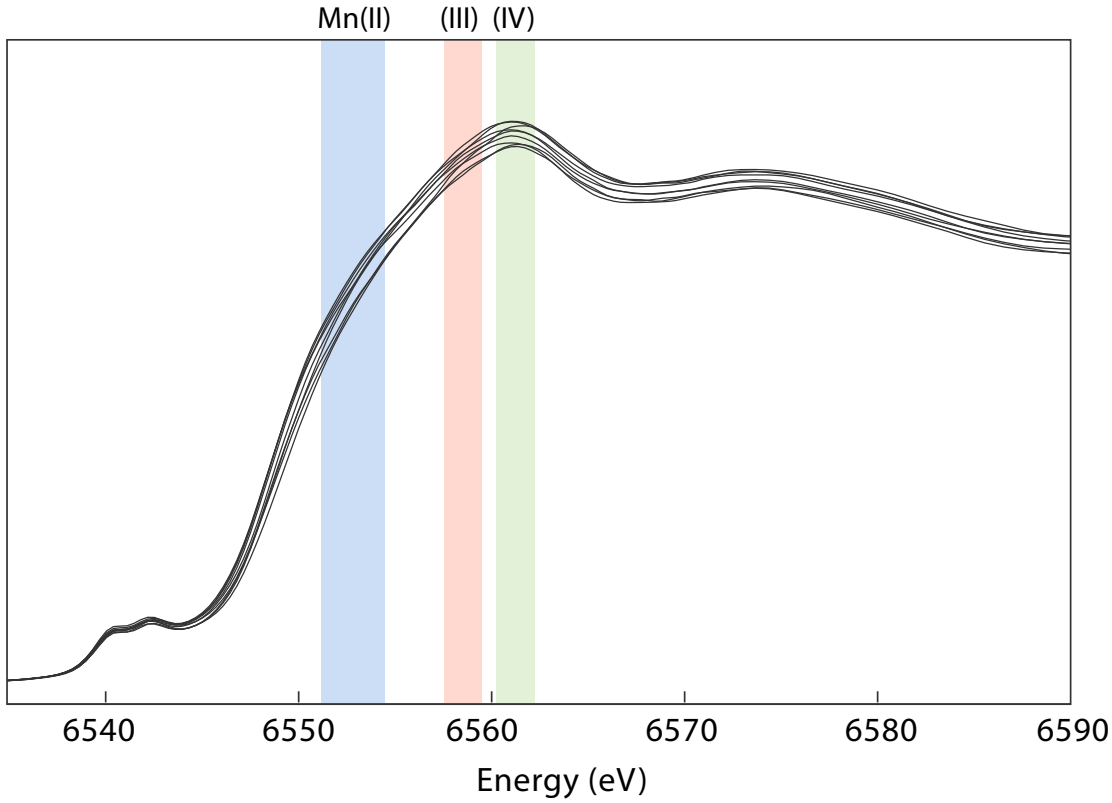

Figure S1 – Control reaction, showing > 5 hours of Mn X-ray absorption spectra with colloidal MnO_2 and 20mM lactate are in solution. Unchanging spectra indicate that there is no perceptible abiotic reaction between colloidal MnO_2 and lactate in a multi-hour time frame and no clear X-ray beam reduction of manganese.

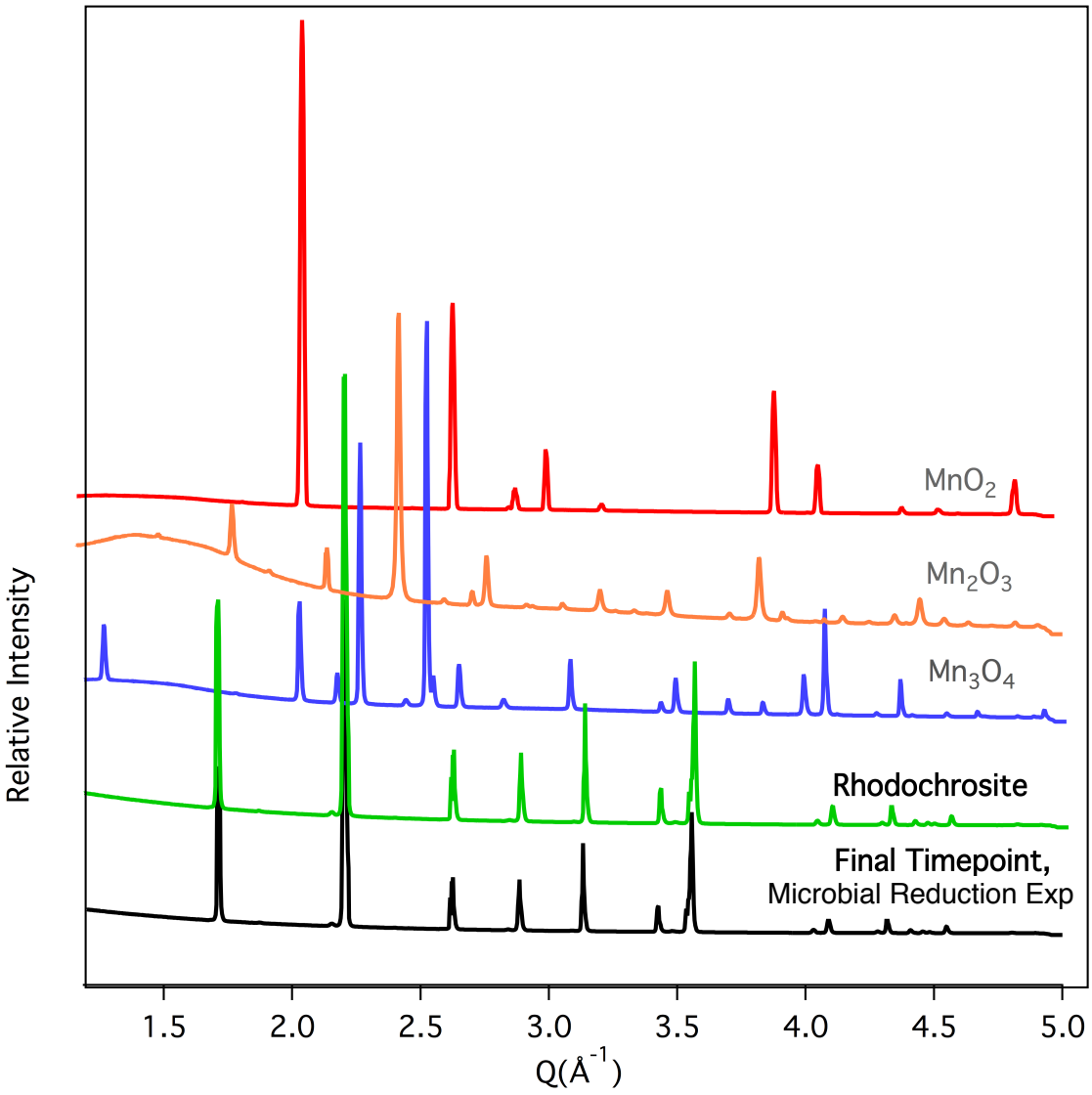

Figure S2 – X-ray diffraction data comparing manganese standards to the final crystalline product of manganese oxide reduction by *S. oneidensis* using lactate (20mM).